

The mechanism for the controlled synthesis of highly dispersed vanadia supported on silica SBA-15

Christian Hess *, Ute Wild, Robert Schlögl

Fritz Haber Institute of the Max Planck Society, Department of Inorganic Chemistry, Faradayweg 4-6, D14195 Berlin, Germany

Received 30 March 2006; received in revised form 6 June 2006; accepted 8 June 2006

Available online 20 July 2006

Abstract

The mechanism for the controlled synthesis of highly dispersed vanadia supported on mesoporous silica SBA-15 ($\text{VO}_x/\text{SBA-15}$) is elucidated using X-ray photoelectron spectroscopy (XPS), Raman and diffuse reflectance infrared Fourier-transform spectroscopy (DRIFTS). The synthesis consists of functionalization of SBA-15 using 3-aminopropyltrimethoxysilane (APTMS) followed by HCl treatment, anion exchange of decavanadate ($\text{V}_{10}\text{O}_{28}^{6-}$) and calcination to yield the final material. Spectroscopic analysis yields that APTMS is grafted onto the surface via hydroxyl groups. Under ambient conditions, protonated APTMS on SBA-15 is largely hydrolyzed and present in its bidentate and tridentate form. Detailed XPS analysis reveals a strong influence of surface water on the resulting structure of APTMS on SBA-15. Under dry conditions, the protonated APTMS molecules on SBA-15 adopt the monodentate and bidentate form. During the anion exchange reaction, decavanadate is incorporated intactly into the pores, without any changes in the structure of the organic framework. In the calcination step, decavanadate is decomposed and vanadia is anchored onto the surface of SBA-15 via silanol groups resulting in highly dispersed surface vanadia species, while the organic residues are fully removed from the pores of the silica matrix.

© 2006 Elsevier Inc. All rights reserved.

Keywords: Supported vanadium oxide; Vanadia; SBA-15; XPS; Vibrational spectroscopy

1. Introduction

Silica SBA-15 is a mesoporous molecular sieve, which possesses uniform hexagonal channels ranging from 5 to 30 nm and a very narrow pore-size distribution [1]. Its large internal surface area ($>800 \text{ m}^2/\text{g}$) allows for the dispersion of a large number of catalytically active centers, whereas its thick framework walls (3.1–6.4 nm) provide high hydrothermal stability that exceeds those of the thinner-walled MCM-41 materials [1–3]. On account of its well-defined structure and variability of the pore diameter, SBA-15 is ideally suited as support material for the preparation of three-dimensional model catalysts. Furthermore, it opens the possibility to study catalysis on well-defined, spatially separated transition metal centers. Despite its great poten-

tial use for catalytic applications, there have been only few reports on the preparation and application of SBA-15 supported vanadium oxide catalysts [4–9].

Vanadium oxides supported on silica exhibit high activity and selectivity for a number of model oxidation reactions, such as the partial oxidation of methane [10,11], methanol oxidation to formaldehyde [8,12–14], and the oxidative dehydrogenation of ethane to ethylene [15]. To understand the correlation between structural and catalytic properties of dispersed vanadia, various techniques including infrared [16–18a,18b], Raman [19–23], UV–visible [16,17,20,24,25], solid-state ^{51}V NMR [21], and X-ray absorption spectroscopy [18,26] have been used. In several studies, XPS has been employed to study the dispersion and oxidation state of supported vanadia catalysts [27,28].

One of the main goals of heterogeneous catalysis is to establish structure–activity relationships. However, controlled synthesis of catalytic materials with active sites,

* Corresponding author. Tel.: +49 30 8413 4500; fax: +49 30 8413 3155.
E-mail address: hess@fhi-berlin.mpg.de (C. Hess).

which are uniform in composition and distribution, is still a challenge. A promising strategy to produce uniform active sites on the surface of an oxide support is based on grafting of an organometallic precursor species followed by its transformation into an active site by chemical reactions [29–31]. Recently, supported vanadia catalysts have been prepared based on grafting of a tailored single-source tri(alkoxy)siloxy precursor compound onto the surface of mesoporous silica followed by thermal decomposition of the precursor [29,32]. Employing spectroscopic techniques such as infrared, UV–Vis, Raman, NMR, and EXAFS, the formation of the adsorbed precursor and the final catalyst were characterized [32]. By using molecular designed dispersion (MDD) of $\text{VO}(\text{acac})_2$, highly dispersed VO_x species have been grafted onto SBA-15 [6]. In this study, the structure of the adsorbed $\text{VO}(\text{acac})_2$ precursor and the final catalyst have been studied using FTIR, Raman spectroscopy and thermogravimetric analysis (TGA), respectively.

In a previous publication we have shown that highly dispersed vanadia supported on SBA-15 can be prepared by a novel grafting/anion exchange method, which consists of organofunctionalization of SBA-15 using APTMS, subsequent anion exchange of decavanadate into the pores of the silica matrix and thermolysis of the precursor material [33]. As the precursor is tightly held electrostatically within the channels in a prearranged geometry, this approach allows for a precise control of the amount of vanadium introduced into the material. Raman and diffuse reflectance UV–Vis spectroscopy under dehydrated conditions revealed the presence of different vanadia structures (monomers, polymers and crystals) as a function of vanadium loading (0–22 wt% V). Therefore, by variation of the loading the structural properties of the resulting vanadia phase can be controlled.

The functionalization of silica using 3-aminopropyltriethoxysilane (APTS), which largely resembles the first step of our procedure, has been studied extensively using various spectroscopic techniques such as infrared, solid-state NMR, TGA and XPS [34,35]. These studies have shown that the presence of surface water strongly influences the resulting structure of the adsorbed APTS [36]. Depending on the amount of water exposure during the modification stages of silica (pretreatment, reaction, curing), different structures were formed. Extensive exposure to water resulted in the formation of an aminopropyl-polysiloxane layer. In contrast, by application of dry conditions during all modification stages the hydrolysis of ethoxy groups could be prevented.

In this article we present a detailed spectroscopic characterization of the synthesis of highly dispersed vanadia supported on silica SBA-15. XPS as well as vibrational spectroscopies, i.e. DRIFTS and Raman, are used to elucidate the chemical composition and structure at the surface of silica SBA-15 after each modification stage. This allows us to propose a detailed mechanism for the formation of $\text{VO}_x/\text{SBA-15}$ based on results from various spectroscopic techniques. Here, we focus on the synthesis of a $\text{VO}_x/\text{SBA-15}$ catalyst with a loading of 2.7 wt% V. This vanadia

loading was chosen because it is well below loadings, at which formation of V_2O_5 crystals was observed (9 wt% V) [33]. Recently, this material was shown to exhibit an excellent catalytic performance in methanol partial oxidation to formaldehyde and propane partial oxidation to acrylic acid [8,9].

2. Experimental

2.1. Material preparation

Silica SBA-15 was synthesized according to the literature [1]. The resulting white powder was calcined at 550 °C for 12 h to obtain the final product. Details of the catalyst preparation were described elsewhere [33]. Briefly, the functionalization of SBA-15 was achieved by stirring 2.5 g SBA-15 in 100 ml of toluene at 65 °C [37]. To this suspension, 6.5 g 3-aminopropyltrimethoxysilane (APTMS) was added while stirring. After stirring for 12 h, the contents was filtered and washed with toluene. This dry, white powder (APTMS-SBA-15) was stirred in 150 ml 0.3 M HCl for 12 h. The contents was filtered again, washed with water and dried in air overnight. SBA-15 supported vanadia was synthesized using functionalized SBA-15 and butylammonium decavanadate, $[\text{H}_3\text{NC}_4\text{H}_9]_6\text{V}_{10}\text{O}_{28}$, (deca) as starting material [38]. For a 2.7 wt% V catalyst, 73 mg of butylammonium decavanadate were added to a suspension of 1 g functionalized SBA-15 in 40 ml water. The contents was stirred for 12 h, filtered, washed with water and dried in air, yielding an orange powder (deca-SBA-15). The powder was calcined at 550 °C for 12 h to yield the final supported vanadia catalyst ($\text{VO}_x/\text{SBA-15}$).

2.2. Physical characterization

The actual composition of the sample was determined by atomic absorption after the samples were dissolved in HF solution. Surface areas of the prepared samples were measured by nitrogen adsorption/desorption isotherms using a Quantasorb surface area analyzer and standard multipoint BET analysis methods. The samples were pretreated overnight in a vacuum line. SBA-15 and $\text{VO}_x/\text{SBA-15}$ were pretreated at 200 °C, APTMS-SBA-15 and deca-SBA-15 at 85 °C, respectively. The deca sample was pretreated overnight in helium at room temperature and measured on a Quantasorb Jr. The pore volume was determined from the adsorption branch of the N_2 isotherm curve at the $P/P_0 = 0.95$ signal point. The pore-size distribution was determined from the desorption branch of the isotherm using the BJH method. Transmission electron microscopy (TEM) was performed using a Philips CM 200 LaB₆ at an acceleration voltage of 200 kV.

2.3. X-ray photoelectron spectroscopy (XPS)

The measurements were carried out using a modified LHS/SPECS EA200 MCD system equipped with a Mg K_α

source (1253.6 eV, 168 W). Spectra were run in both low-resolution (retardation ratio 4) and high-resolution (pass energy 48 eV) modes. X-ray satellites were removed numerically. The binding energy scale of the system was calibrated using $\text{Au } 4f_{7/2} = 84.0$ eV and $\text{Cu } 2p_{3/2} = 932.67$ eV from foil samples. The powder samples were placed as is in a stainless steel sample holder with a 0.6 mm deep rectangular well covering an area of (12×8) mm². The base pressure of the ultra-high vacuum (UHV) chamber was 1×10^{-10} mbar. The position of the sample holder in the analysis chamber could be well reproduced allowing a good comparison of absolute intensities of different samples. Unless noted differently the acquisition time was 260 min. Charging of the powder samples was accounted for by setting the peak of the Si 2p signal to 103.6 eV [39]. A Shirley background was subtracted from all spectra. Then peak fitting with a 30/70 Gauss–Lorentz product function was performed. Atomic ratios were determined from the integral intensities of the signals, which were corrected by empirically derived sensitivity factors [40].

2.4. Raman spectroscopy

The Raman spectrometer (Kaiser Optical) was equipped with a Nd:YAG laser which was frequency doubled to 532 nm. The laser was operated at a power level of 25 mW measured at the sample using a power meter (Coherent). The spectral resolution of the spectrometer was 5 cm^{-1} . To minimize the effect of laser heating the samples (~ 50 mg) were pressed into pellets at 40 MPa and rotated at 20 Hz within a rotary quartz Raman cell. Sampling times were between 100 and 200 s. All Raman spectra were recorded under ambient conditions unless stated otherwise. The Raman spectra of the dehydrated vanadia samples were recorded at room temperature after heating the samples in flowing air at 400 °C for 1 h.

2.5. Diffuse reflectance infrared Fourier-transform spectroscopy (DRIFTS)

DRIFT spectra were recorded on a Bruker IFS 66 spectrometer, with 4 cm^{-1} spectral resolution, equipped with a Graseby Specac diffuse reflectance accessory, after diluting the samples with 90% of oven-dried KBr. The sampling time was 1000 s. All spectra were recorded under ambient conditions. Spectra were normalized by using the 1770–1940 cm^{-1} Si–O band as a reference.

3. Results and discussion

3.1. Synthesis of $\text{VO}_x/\text{SBA-15}$

Fig. 1 depicts XP survey spectra, which highlight important steps of the synthesis of 2.7 wt% V/SBA-15. Detailed high-resolution XP spectra of the corresponding compounds will be discussed below. The atomic ratios of the detected elements, as obtained from the XPS analysis, as well as their BET surface area values are listed in Table

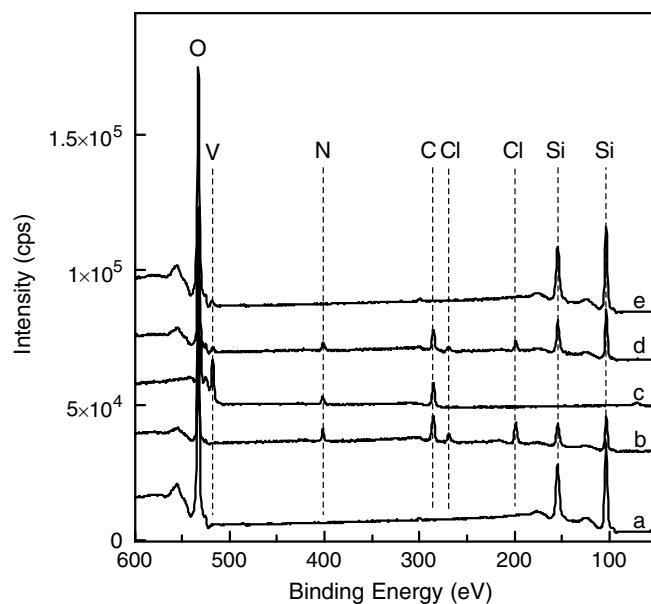


Fig. 1. XP survey spectra of (a) SBA-15, (b) APTMS-SBA-15, (c) deca, (d) deca-SBA-15, and (e) 2.7 wt% V/SBA-15. The spectra are offset for clarity.

1. Parts (a) and (b) of Fig. 1 show the spectra of untreated SBA-15 and APTMS-SBA-15, which has been functionalized with APTMS and subsequently treated with HCl. As indicated in Fig. 1, the spectrum of SBA-15 is characterized by Si 2s, Si 2p and O 1s peaks. The spectrum of APTMS-SBA-15 exhibits peaks corresponding to C 1s, N 1s, Cl 2s and Cl 2p, in addition to the SBA-15-related Si and O peaks. The N/C and N/Cl ratios (see Table 1) suggest the presence of the ammonium salt of APTMS on the surface of SBA-15 (see discussion below). The Si 2s and Si 2p peaks of SBA-15 and APTMS-SBA-15 appear at the same binding energy, which indicates that Si from silane is indistinguishable from Si in SBA-15. Part (c) displays the X-ray photoelectron spectrum of butylammonium decavanadate (deca), which serves as vanadium precursor in the synthesis of $\text{VO}_x/\text{SBA-15}$. The observed peaks correspond to O 1s, V 2p, C 1s, and N 1s. The values for the atomic ratios given in Table 1 confirm the presence of intact butylammonium decavanadate. However, the O/V ratio of 2.4 (expected: 2.8) indicates that the sample is slightly reduced (see discussion below). Part (d) of Fig. 1 shows the spectrum of deca-

Table 1

BET results and atomic ratios (%) of the detected elements as obtained from the XPS analysis

	Na 1s	O 1s	V 2p _{3/2}	N 1s	C 1s	Cl 2p	Si 2p	S_{BET} (m ² /g)
SBA-15	0	70.2	0	0	0	0	29.8	826
APTMS-SBA-15	3.9	39.0	0	5.8	25.7	5.1	20.5	70
Deca	0	36.7	15.2	8.3	39.8	0	0	1.5
Deca-SBA-15	1.2	50.6	0.9	4.0	17.1	2.2	24.0	48
$\text{VO}_x/\text{SBA-15}$	0	68.3	0.7	0	0	0	31.0	445

SBA-15, which was obtained from APTMS-SBA-15 by anion exchange with decavanadate. The presence of the $V2p_{3/2}$ peak and the slight increase of the O1s intensity are indicative of the presence of decavanadate in the pores of the silica matrix. Moreover, the decrease in the Cl/N ratio when going from APTMS-SBA-15 to deca-SBA-15 clearly demonstrates that anion exchange has taken place. On the basis of the resulting V/N ratio of 0.22, which results in the formation of 2.7 wt% V/SBA-15, the upper limit for loading SBA-15 with vanadia using the above procedure can be determined as 20.5 wt% V/SBA-15. This result is in excellent agreement with the experimentally determined value (22 wt% V) for the saturation loading [33]. Furthermore, it demonstrates the potential of this approach to precisely control the amount of vanadium introduced into SBA-15 over a broad range of vanadia loadings. The survey spectrum of deca-SBA-15 resembles that of APTMS-SBA-15, which suggests that the organic matrix has not been modified during the incorporation of decavanadate as discussed in more detail below. This is illustrated by the N/C ratio, which was observed to be comparable before and after the anion exchange reaction (see Table 1). In part (e), the spectrum of the final catalyst, 2.7 wt% V/SBA-15, is shown. Besides the presence of the V2p peaks (see Fig. 6 for detailed $V2p_{3/2}$ XPS spectra), the spectrum resembles that of part (a) as far as position and intensity of the observed peaks are concerned. Note that no carbon peak was observed for VO_x /SBA-15, which indicates that during the calcination step essentially all organic residues were removed. Besides this, neither chlorine nor sodium was detected in the final material by XPS. The nitrogen isotherms of SBA-15, deca-SBA-15 and VO_x /SBA-15 are shown in Fig. 2. All isotherms are

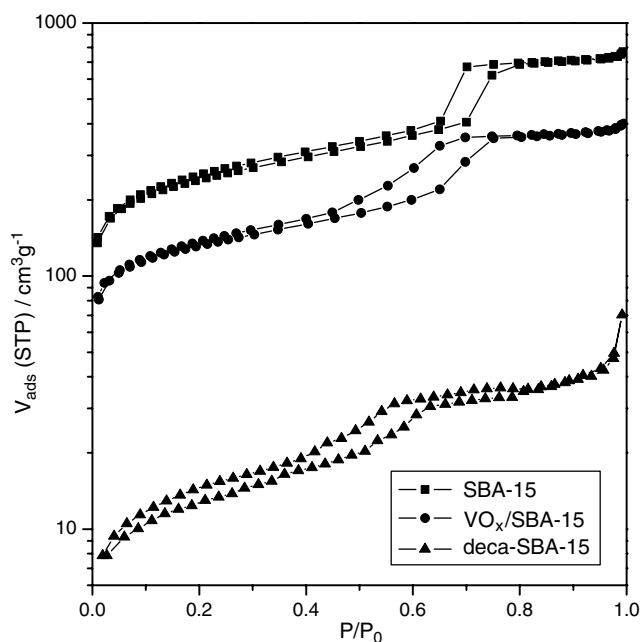


Fig. 2. N_2 isotherms of SBA-15, deca-SBA-15 and 2.7 wt% V/SBA-15.

Table 2
BET characteristics of the synthesized SBA-15 supported vanadium oxide compared to the blank SBA-15 support

	V (wt%)	V (nm^2)	V (mmol/g)	S_{BET} (m^2/g)	r_p (nm)	V_p (mL/g)
SBA-15	0.0	0.0	0.0	826	3.58	0.72
VO_x /SBA-15	2.7	0.7	0.53	445	3.26	0.43

of type IV exhibiting a H1-type hysteresis loop, which is typical of mesoporous materials. The results of the physisorption characterization reveal pore diameters of 7.16 and 6.52 nm for SBA-15 and the VO_x /SBA-15 (see Table 2), respectively, as well as a value of 4.75 nm for the modified surface (deca-SBA-15). With vanadia loading, the surface area, pore radius and pore volume shift to lower values. However, BET reveals that in the presence of vanadium oxide the mesoporous channels remain accessible. Previously we have shown that the pore radius and pore volume decrease significantly with vanadium loading which suggests that the vanadia species are located inside the pores of SBA-15, coating the inner walls of the mesoporous matrix [33]. As indicated by X-ray diffraction and TEM (not shown) of the final VO_x /SBA-15 material, the pore structure of SBA-15 is conserved throughout the synthesis [33,9].

3.2. XPS

3.2.1. APTMS-SBA-15

Fig. 3 shows the high-resolution C1s (left panel) and N1s (right panel) spectra of APTMS-SBA-15 together with the results from the peak-fitting procedure. Table 3 summarizes the binding energies, FWHM, and fractions of the corresponding peaks. The C1s peaks at 286.8 eV (26.4%) and 288.7 eV (4.3%) are assigned to carbon bound to a single oxygen and bicarbonate-type carbon, respectively. The other forms of carbon are represented by a peak at 285.4 eV (69.3%). The fact that some bicarbonate-type carbon is observed although none was expected is indicative of the interaction of APTMS grafted onto the silica surface with CO_2 and H_2O which leads to the formation of a bicarbonate salt ($R-NH_3^+HCO_3^-$) according to Eq. (1) [41]:



Therefore, the peak at 288.7 eV is assigned to bicarbonate. The contribution of carbonyl-type carbon in APTMS-SBA-15 amounts to 1.1% (see Tables 1 and 3). Therefore, based on the C/N ratio for bicarbonate of 1, 22% of the total amount of nitrogen present as NH_3^+ is formed according to Eq. (1). The C–O peak at 286.8 eV is assigned to methoxy, in agreement with reported C1s binding energies for alkoxy groups bound to Si [42]. Based on the fit results, the ratio of propyl carbon (C–C) to nitrogen was determined as 3.07. This result nicely demonstrates that the sample was essentially free from carbon impurities.

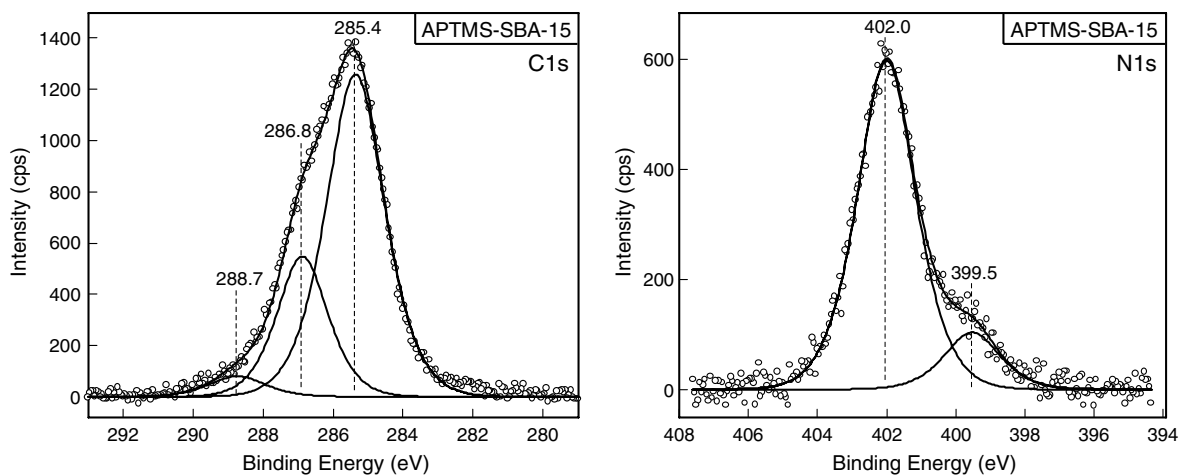


Fig. 3. XP C 1s (left panel) and XP N 1s (right panel) spectra of APTMS-SBA-15 together with the results from the peak-fitting procedure.

Table 3
Results from the analysis of the high-resolution XPS spectra

		C 1s			N 1s		V 2p _{3/2}	
		C–C	C–O	HCO ₃ [−]	NH ₂	NH ₃ ⁺	V ³⁺	V ⁵⁺
APTMS-SBA-15	BE	285.4	286.8	288.7	399.5	402		
	FWHM	2.2	1.9	2.1	2.1	2.2		
	%	69.3	26.4	4.3	14.3	85.7		
Deca-SBA-15	BE	285.3	286.6	288.0	400.2	402.2	515.9	517.2
	FWHM	2.3	1.9	2.2	2.7	2.2	2.3	2.3
	%	71.6	21.4	7	72.2	27.8	46.8	53.2
260 min	BE	285.3	286.6	288.0	400.2	402.2	515.9	517.2
	FWHM	2.3	1.9	2.4	2.5	2.4	2.3	2.3
	%	70.8	19.5	9.7	39.9	60.1	20.6	79.4
VO _x /SBA-15	BE						515.9	517.3
	FWHM						2.2	2.0
	%						24.1	75.9

The binding energy (BE/eV), FWHM (eV), and fraction (%) given were determined from the integrals of the Gauss–Lorentz fit functions shown in Figs. 3–6.

Previous studies on 3-aminopropyltriethoxysilane (APTS) adsorption on hydrated amorphous silica have shown that the APTS molecules are predominantly in their bidentate and tridentate form (with two and three Si–O–Si bonds, respectively) [34]. Also the contribution from non-hydrolyzed monodentate was found to be small, while the hydrolyzed monodentate form was absent. Based on steric reasons it was concluded that three covalent bonds with the surface can be excluded implying polymerization of tridentate APTS. From the results of the area fits, the ratio of carbon bound to oxygen (C–O) to nitrogen was determined as 1.17. These XPS results show that the majority of APTS molecules were in their bidentate form with a contribution from monodentate APTS. Previously, the influence of surface water in the reaction of APTS with silica gel was studied extensively using ²⁹Si NMR and DRIFTS [36]. It was shown that hydrolysis of the alkoxy groups was prevented and mainly bidentate but no polymerized (tridentate) APTS was formed, when all modification stages, the silica pretreatment, the reaction of silica with APTS, as well

as the curing stage were performed under dry/vacuum conditions. Although the present experiments were conducted under comparable conditions as above, an additional reaction step, the formation of the ammonium salt of APTS, was performed before the sample was dried and examined with XPS. As this reaction was conducted in (aqueous) HCl solution, the presence of a small amount of tridentate APTS cannot be excluded.

The right panel of Fig. 3 displays the N 1s spectrum of APTMS-SBA-15. The peak consists of two components centered at 399.5 eV and 402.0 eV. In agreement with the literature, the former is attributed to the free amine group (R–NH₂) and the latter is attributed to a protonated amino group (R–NH₃⁺) [41,43]. Quantitative analysis of the N 1s peak yields that 85.7% of the amine is present in its protonated form and 14.3% as free amine (see Table 3). As can be seen from Table 1, the amount of NH₃⁺ closely matches the amount of chlorine as would be expected from the formation of the ammonium chloride. Previous work on alkylamine-silanized metal oxides has shown that some

nitrogen, which is present in form of amine (NH_2), resists protonation in acid solution [44]. It has been suggested that these amino groups are associated with hydrogen bonding between amino groups and surface hydroxyl. On the other hand, amine protonated while in contact with the acid solution is possibly deprotonated when dried or placed in vacuum, which results in a decreased ratio $\text{NH}_3^+/\text{NH}_2$. In experiments in which the exposure time was reduced to 30 min (compared to 260 min), a slightly higher fraction of NH_3^+ of 89.3% (compared to 85.7%) was obtained, indicating that the influence of the analysis conditions on the ratio $\text{NH}_3^+/\text{NH}_2$ was only minor for this sample.

3.2.2. Deca-SBA-15

The C1s XP spectrum (not shown) of deca-SBA-15 strongly resembles that of APTMS-SBA-15. The C1s peak consists of three components which are centered at 285.3 eV (71.6%), 286.6 eV (21.4%), and 288.0 eV (7%) (see Table 3). As discussed above, they can be assigned to carbon, which is part of the propyl chain (C–C), carbon bound to a single oxygen atom (C–O), and bicarbonate-type carbon, respectively. Based on the ratio of propyl carbon (C–C) to nitrogen of 3.05, there is no indication for the presence of carbon impurities. However, a slightly different intensity distribution is observed indicating chemical transformations within the organic framework during the anion exchange reaction. For deca-SBA-15, the ratio of methoxy carbon (C–O) to nitrogen was determined as 0.91, which suggests that the majority of APTMS was present in its bidentate form. By comparison with the higher C/N ratio of 1.17 obtained for APTMS-SBA-15, this result implies the hydrolysis of part of the methoxy groups. However, based on the XPS results, a contribution from polymerized APTMS cannot be ruled out, as previous experiments have shown an increase in the amount of polymerized silane molecules with increasing exposure to water during the modification of silica with APTS [34].

Fig. 4 depicts N1s XP spectra of deca-SBA-15. They were obtained after exposure of the sample to the X-ray beam for 30 min and 260 min, respectively. Both spectra can be described by a sum of two components centered at 400.2 and 402.2 eV. As discussed above, they are attributed to the free amine group (NH_2) and to a protonated amino group (NH_3^+), respectively. After 30 min of exposure, significantly more NH_3^+ (60.1%) than NH_2 (39.9%) was observed. Clearly, longer exposure times lead to a strong decrease of the ratio $\text{NH}_3^+/\text{NH}_2$ from 1.51 to 0.39. This is indicative of a conversion of NH_3^+ into NH_2 as result of the measurement process, i.e. the X-ray beam and/or vacuum. Such a pronounced alteration of the protonated amino group was only observed in case of the deca-SBA-15 sample, whereas APTMS-SBA-15 was much more stable.

Detailed XPS spectra of the V2p region of deca-SBA-15 are shown in Fig. 5. Fig. 5 depicts spectra of deca-SBA-15 after exposure to the X-ray beam for 30 min (bottom) and 260 min (top) together with the spectrum of blank SBA-15.

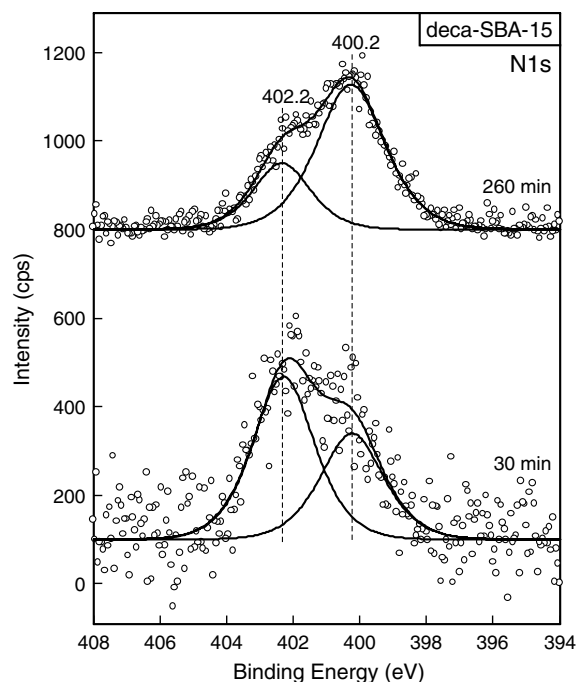


Fig. 4. XP N1s spectra of deca-SBA-15 after 30 min and 260 min together with the results from the peak-fitting procedure. The spectra are offset for clarity.

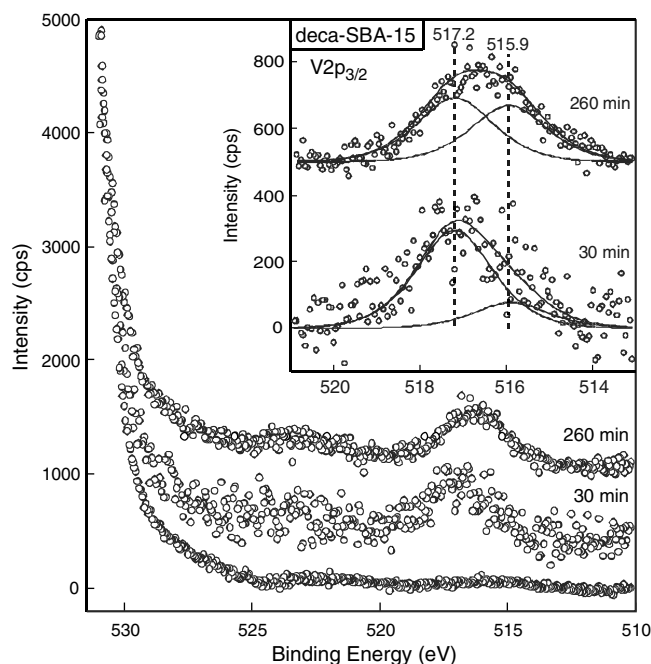


Fig. 5. XP spectra of deca-SBA-15 after 30 min and 260 min (upper curves) and blank SBA-15 (lower curve). The $\text{V}2\text{p}_{3/2}$ region of the resulting difference spectra is shown as inset together with the results from the peak-fitting procedure. For details see text.

As the spectrum of SBA-15 shows structure in the V2p region, it was used for background subtraction. The resulting spectra of the $\text{V}2\text{p}_{3/2}$ region are shown as inset of

Fig. 5. Both spectra can be described as the sum of two components centered at 517.2 eV (A) and 515.9 eV (B). The position of component A agrees well with the $V2p_{3/2}$ binding energy we have observed for V_2O_5 , in which vanadium is expected to be in its highest oxidation state (+5). Therefore, we attribute component A to the V^{5+} oxidation state. As the *absolute* values of the binding energies of vanadium in all oxidation states vary significantly in the literature, the assignment of component B was based on the reported *differences* in the binding energies, ΔBE , of V^{5+} and lower oxidation states. Generally, the reported ΔBE between V^{5+} and V^{4+} is 0.7–1.0 eV, and the reported ΔBE between V^{5+} and V^{3+} is 1.2–1.5 eV [27,28,43,45,46]. This suggests that component B corresponds to V^{3+} . Quantitative analysis of the $V2p_{3/2}$ peak yields that 53.2% of the total V is present as V^{5+} and 46.8% is present as V^{3+} . It is mentioned in the literature that prolonged exposure to X-rays can lead to a reduction of vanadium oxides [47]. Here, the reduction of decavanadate incorporated into SBA-15 (deca-SBA-15) is directly observed while the organic framework stays intact (see Table 3). When exposing the sample to X-rays for 260 min, the reduction of vanadium is accompanied by a color change from orange to green. The green color is characteristic for V^{3+} in aqueous solution and points to the presence of water on the surface of deca-SBA-15. On the other hand, it is well known that vanadium retains its oxidation state (5+) in air. The observed V^{3+} contribution to the $V2p_{3/2}$ peak can therefore be attributed to the reduction of V^{5+} during the XPS measurement. These experiments clearly demonstrate that extreme care has to be taken when XPS is used to determine oxidation states of vanadia catalysts.

3.2.3. $VO_x/SBA-15$

After calcination of the precursor material (deca-SBA-15), the oxidation state of V in the as-synthesized $VO_x/SBA-15$ was investigated using XPS. Fig. 6 depicts detailed XP spectra of the V2p region of 2.7 wt% V/SBA-15 together with that of blank SBA-15. As explained above, the spectrum of SBA-15 shows was used for background subtraction. The resulting spectrum of the $V2p_{3/2}$ region is shown as inset of Fig. 6. Its peak can be described by two components centered at 517.3 eV and 515.9 eV, which are assigned to V^{5+} and V^{3+} , respectively. As discussed above, the observed V^{3+} contribution to the $V2p_{3/2}$ peak is attributed to the reduction of V^{5+} during the XPS measurement. Quantitative analysis yields that for $VO_x/SBA-15$ 75.9% of the total V is present as V^{5+} and 24.1% is present as V^{3+} (see Table 3). These results show that the $VO_x/SBA-15$ sample is more stable regarding the reduction of V^{5+} as deca-SBA-15.

3.3. Raman

Fig. 7 shows a series of low-frequency Raman spectra obtained during the synthesis of 2.7 wt% V/SBA-15. As discussed previously [33], the spectrum of blank SBA-15

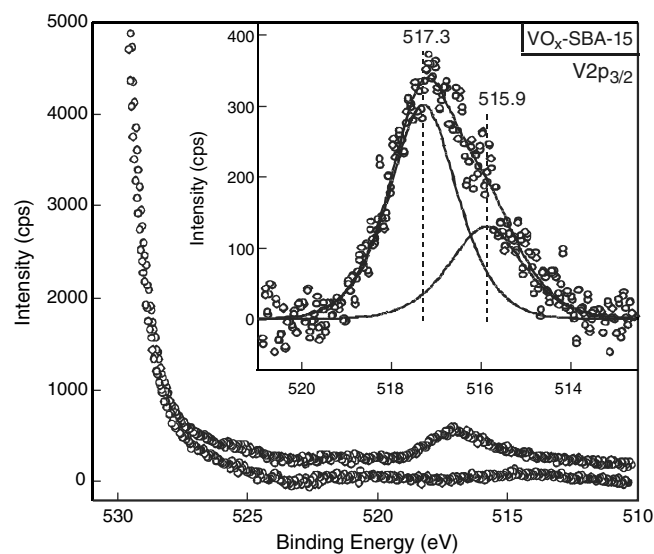


Fig. 6. XP spectra of 2.7 wt% V/SBA-15 (upper curve) and blank SBA-15 (lower curve). The $V2p_{3/2}$ region of the resulting difference spectrum is shown as inset together with the results from the peak-fitting procedure. For details see text.

(spectrum (a)) shows Raman features around 485 and 977 cm^{-1} , which are attributed to cyclic tetrasiloxane rings of the silica support (D1 defect mode) [48] and the Si–OH stretching vibration of surface hydroxyl groups [49], respectively. In addition, weaker Raman bands appeared around 600 cm^{-1} and 810 cm^{-1} , which are assigned to cyclic trisiloxane rings (D2 defect mode) and the symmetrical Si–O–Si stretching mode, respectively [49]. Functionalization of SBA-15 with APTMS and subsequent transformation into the ammonium salt leads to the appearance of new major bands at 940 and 1040 cm^{-1} , respectively (spectrum (b)).

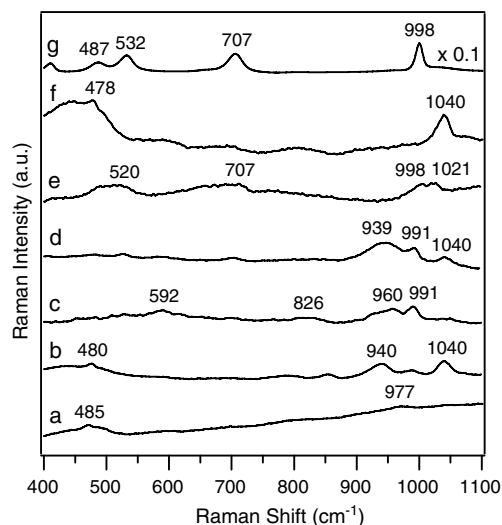


Fig. 7. Raman spectra showing the low-frequency region of (a) SBA-15, (b) APTMS-SBA-15, (c) deca, (d) deca-SBA-15, (e) 2.7 wt% V/SBA-15 under ambient conditions, (f) dehydrated 2.7 wt% V/SBA-15, and (g) crystalline V_2O_5 . The spectra are offset for clarity.

stretch vibrations of the propylammonium group, respectively [50,51]. Spectrum (c) corresponds to deca, which shows Raman bands at 592, 826, 960 and 991 cm^{-1} , respectively, in good agreement with those reported for sodium decavanadate ($\text{Na}_6\text{V}_{10}\text{O}_{28} \cdot 18\text{H}_2\text{O}$) [52]. The spectrum of deca-SBA-15, spectrum (d), is characterized by Raman bands at 596, 939, 991 and 1040 cm^{-1} , respectively. Qualitatively, spectrum (d) can be considered as a superposition of spectra (b) and (c). As discussed above and also confirmed by Raman spectra of the high-frequency region of deca (see Fig. 8), the functionalized SBA-15 is unaffected by the anion exchange. These results demonstrate that Raman spectroscopy allows for the unambiguous identification of decavanadate in the pores of the silica matrix, as its vibrational signature is distinctly different from that of other vanadia compounds, e.g. V_2O_5 (see spectrum (g)). Thermal decomposition of deca-SBA-15 yields the product of the synthesis, 2.7 wt% V/SBA-15. Its Raman spectrum (see spectrum (e)) clearly differs from that of deca-SBA-15 and shows bands at 520, 656, 707, 998 and 1021 cm^{-1} , respectively. Previously, similar bands were assigned to hydrated surface vanadium oxide species forming a $\text{V}_2\text{O}_5 \cdot n\text{H}_2\text{O}$ gel due to the close resemblance with the Raman bands observed for $\text{V}_2\text{O}_5 \cdot n\text{H}_2\text{O}$ xerogel [53]. Raman spectrum (f) corresponds to 2.7 wt% $\text{VO}_x/\text{SBA-15}$ after dehydration. It is dominated by a $\text{V}=\text{O}$ stretching band at 1040 cm^{-1} , which has been assigned to vanadium in a tetrahedral coordination [15,17–20]. No V_2O_5 -related bands (see spectrum (g) for comparison) were observed demonstrating the highly dispersed state of the anchored vanadium oxide species.

Fig. 8 depicts the high-frequency region of the Raman spectra obtained during the synthesis of 2.7 wt% V/SBA-15. As reference, the spectrum of blank SBA-15 (spectrum (a)) and methoxy adsorbed on SBA-15 (spectrum (c)) are

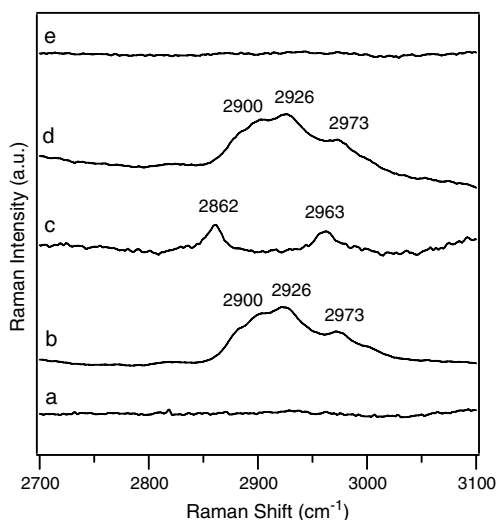


Fig. 8. Raman spectra showing the high-frequency region of (a) SBA-15, (b) APTMS-SBA-15, (c) methoxy adsorbed on SBA-15, (d) deca-SBA-15, and (e) 2.7 wt% V/SBA-15 under ambient conditions. The spectra are offset for clarity.

shown. Methoxy adsorbed on SBA-15 gives rise to two Raman bands at 2862 cm^{-1} and 2963 cm^{-1} , which are characteristic of C–H stretching vibrations of a methoxy group. After grafting of APTMS onto SBA-15 and subsequent formation of the ammonium salt (APTMS-SBA-15) spectrum (b) was obtained. As can be seen from spectrum (b), no major Raman intensity is observed in the region around 2860 cm^{-1} , which suggests that a large fraction of the methoxy groups of APTMS has reacted. Spectrum (b) shows broad bands at ~ 2900 , 2926 and 2973 cm^{-1} , respectively, which are attributed to C–H stretch vibrations of the three CH_2 groups [54]. As each of the methylene groups is in a different chemical environment, we expect the C–H stretch bands to appear at different frequencies. The ion exchange of decavanadate for chloride does not affect the high-frequency region of the spectrum (see spectrum (d)). After the final steps of the synthesis, the thermal decomposition of decavanadate and formation of $\text{VO}_x/\text{SBA-15}$, no high-frequency Raman bands were observed (see spectrum (e)). The absence of C–H-related stretching bands suggests that the grafted ammoniumpropyl is removed during the thermal treatment as confirmed by XPS and DRIFTS (see below).

The last step of the synthesis, i.e. the anchoring of the vanadia precursor to the silica surface during calcination, was also studied using vibrational spectroscopy. Fig. 9 shows visible Raman spectra of the final catalytic material, 2.7 wt% V/SBA-15, and blank SBA-15. They were recorded at room temperature after dehydration in flowing air at 400 $^\circ\text{C}$ for 1 h. The spectrum of blank SBA-15 is characterized by a Raman feature at 980 cm^{-1} , which is attributed to the Si–OH stretch of surface hydroxyl groups, as discussed above. In contrast, the spectrum of 2.7 wt% V/SBA-15 is dominated by the $\text{V}=\text{O}$ stretching band at 1040 cm^{-1} (see above). After loading of vanadia, the hydroxyl band at 980 cm^{-1} is not observed anymore. This

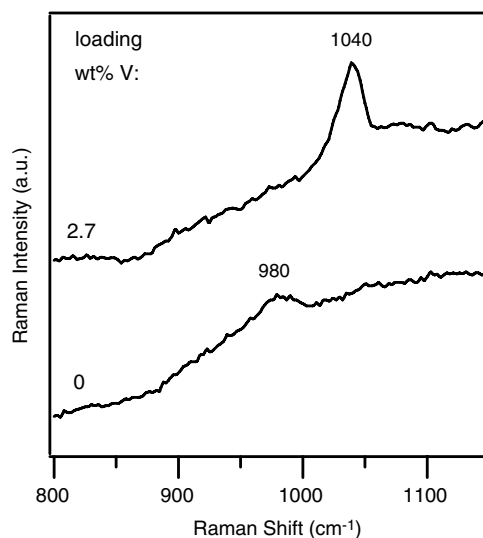


Fig. 9. Raman spectra of dehydrated 2.7 wt% V/SBA-15 and SBA-15. The spectra are offset for clarity.

demonstrates that the vanadia precursor is anchored to the silica support via surface hydroxyl groups. It should be noted that a quantitative analysis is difficult due to the fact that the surface area is significantly reduced in the course of the synthesis of VO_x/SBA-15 (see Table 2).

3.4. DRIFTS

Fig. 10 shows DRIFT spectra of (a) SBA-15, (b) APTMS-SBA-15, (c) deca-SBA-15, and (d) 2.7 wt% V/SBA-15 under ambient conditions. The high-frequency region shows a narrow band at 3746 cm⁻¹, which is assigned to free silanols. The broad band at 3200–3600 cm⁻¹ is attributed to the presence of bridged silanols or physisorbed water trapped in the pores of the silica matrix [34]. The functionalization of SBA-15 with APTMS,

i.e. the formation of APTMS-SBA-15, results in dramatic changes of the DRIFT spectrum. The low-frequency region shows a pattern of infrared bands between 1300 and 1500 cm⁻¹, which are characteristic for APTMS modified silica [34]. The bands at 1392, 1413, 1447 and 1472 cm⁻¹ are attributed to bending vibrations of CH₃, Si-CH₂, CH₃ and CH₂, respectively, while the bands at 2881 and 2938 cm⁻¹ are assigned to CH₂ stretching vibrations. All the above band positions are in excellent agreement with those reported previously [34]. The band at 3046 cm⁻¹ is characteristic of N-H stretching vibrations in NH₃⁺, and the pair of broad bands at 3240 cm⁻¹ and 3410 cm⁻¹ is attributed to N-H stretching vibrations in NH₂ [55]. Spectrum (c) corresponds to deca-SBA-15. It largely resembles spectrum (b) in both parts of the spectrum shown in Fig. 10. This demonstrates that during the anion exchange

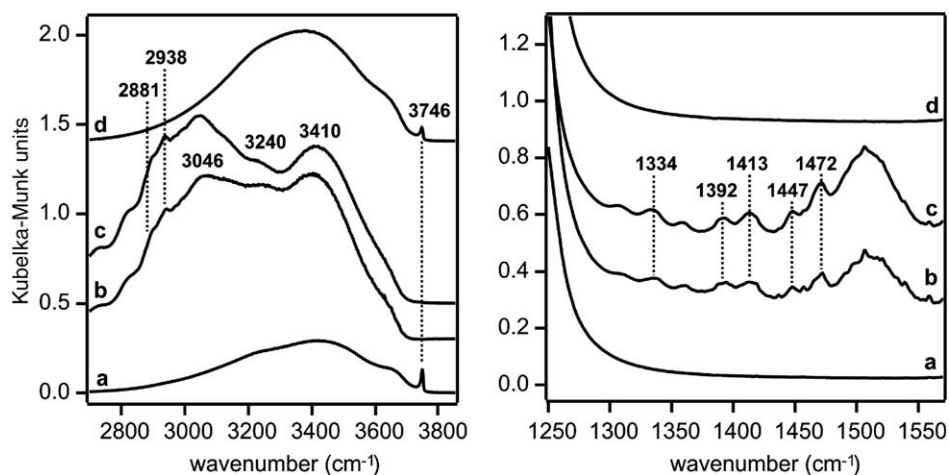
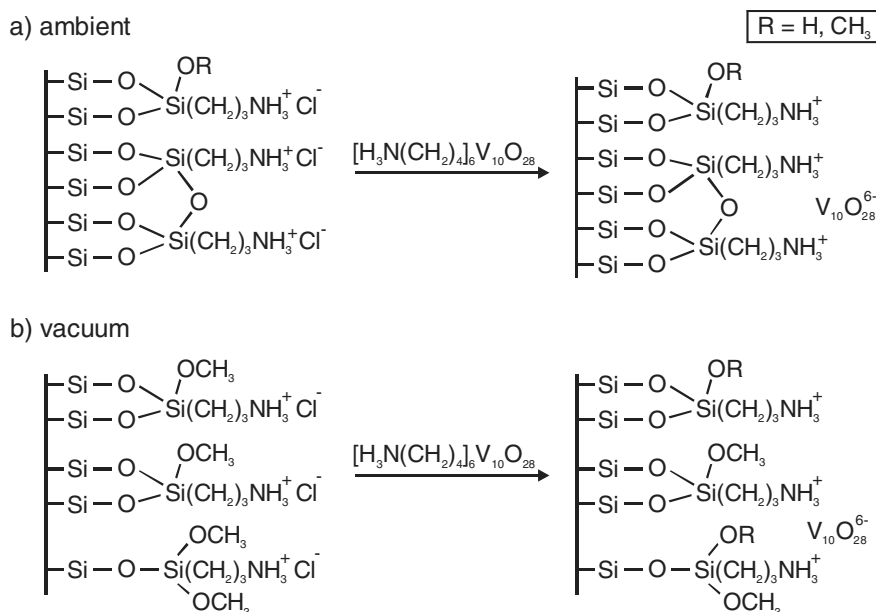


Fig. 10. DRIFT spectra of (a) SBA-15, (b) APTMS-SBA-15, (c) deca-SBA-15, and (d) 2.7 wt% V/SBA-15 under ambient conditions. The spectra are offset for clarity.



Scheme 1. Bonding models of APTMS-SBA-15 and deca-SBA-15 as observed under (a) ambient conditions and (b) vacuum.

reaction no changes in the structure of the organic framework occur, thereby nicely confirming the results from the above XPS and Raman measurements. Spectrum (d) corresponds to the product of the synthesis, VO_x/SBA-15. All vibrations related to the organic framework have disappeared because of thermolysis or oxidation during the calcination step, in excellent agreement with the results from XPS and Raman spectroscopy.

4. Synthesis mechanism

On the basis of the above-mentioned results, the following reaction mechanism is proposed: (1) The surface of SBA-15 is modified via its hydroxyl groups by grafting of 3-aminopropyltrimethoxy-silane (APTMS). Subsequent treatment with HCl results in the formation of the corresponding ammonium salt (APTMS-SBA-15). Under ambient conditions, the protonated APTMS is present in its bidentate and tridentate forms as shown in Scheme 1(a) [56]. In UHV, however, the majority of protonated APTMS molecules adopt the monodentate and bidentate forms (see Scheme 1(b)). (2) During the anion exchange reaction, decavanadate (V₁₀O₂₈⁶⁻) is incorporated intactly into the pores of the silica matrix without structural changes of the organic framework. In vacuum, however, a smaller fraction of methoxy is present in the case of deca indicating partial hydrolysis during the anion exchange reaction (see Scheme 1(b)). (3) Thermal decomposition of the decavanadate precursor material yields the final supported vanadia catalyst (VO_x/SBA-15). During this process, all organic residues as well as chlorine and sodium are completely removed from the pores. Vanadia is anchored onto the surface of SBA-15 via reaction with silanol groups.

5. Conclusions

The synthesis of highly dispersed vanadia supported on mesoporous silica SBA-15 has been studied in detail by using a combination of X-ray photoelectron spectroscopy (XPS) and vibrational spectroscopy. In the first step of the synthesis, APTMS is grafted onto the surface via hydroxyl groups as shown by XPS. Subsequent treatment with HCl solution results in the formation of the corresponding ammonium salt (APTMS-SBA-15) as proven by the C 1s and N 1s XPS spectra. The C–C stretch and C–H stretch bands in the Raman spectrum confirm the presence of the propyl chain. Also, DRIFTS shows a vibrational signature characteristic for APTMS modified silica. The fact that the high-frequency region of the Raman spectrum of APTMS-SBA-15 does not show a major methoxy-related band suggests that under ambient conditions protonated APTMS is present in its bidentate and tridentate (polymerized) forms. XPS analysis revealed a strong influence of surface water on the resulting structure of APTMS. In UHV, i.e. under dry conditions, the protonated APTMS molecules adopt the monodentate and bidentate form.

During the anion exchange reaction, decavanadate is incorporated intactly into the pores as evidenced by the presence of the characteristic V=O stretch Raman band of decavanadate at 991 cm⁻¹. No changes in the structure of the organic framework were observed. However, XPS analysis of deca-SBA-15 reveals a smaller fraction of methoxy compared to APTMS-SBA-15, which is indicative of partial hydrolysis of methoxy during anion exchange. It is shown that calcination yields the final supported vanadia catalyst, while the organic residues as well as chlorine and sodium are fully removed from the pores. The vanadia precursor is grafted onto the surface of SBA-15 via hydroxyl groups as evidenced by the decrease in the Raman intensity of the silanol stretching band.

Acknowledgements

The authors wish to thank Mrs. Anja Hoffmann and Gisela Lorenz for kindly performing the BET measurements and Norbert Pfänder for performing the TEM measurements. C.H. thanks the Deutsche Forschungsgemeinschaft (DFG) for providing an Emmy Noether fellowship.

References

- [1] D.Y. Zhao, J.L. Feng, Q.S. Huo, N. Melosh, G.H. Fredrickson, B.F. Chmelka, G.D. Stucky, *Science* 279 (1998) 548.
- [2] K. Cassiers, T. Linssen, M. Mathieu, M. Benjelloun, K. Schrijnemakers, P. Van der Poort, P. Cool, E.F. Vansant, *Chem. Mater.* 14 (2002) 2317.
- [3] J. Jarupatrakorn, T.D. Tilley, *J. Am. Chem. Soc.* 124 (2002) 8380.
- [4] Y.-M. Liu, Y. Cao, K.-K. Zhu, S.-R. Yan, W.-L. Dai, H.-Y. He, K.-N. Fan, *Chem. Commun.* (2002) 2832.
- [5] H.H. Lopez, A. Martinez, *Catal. Lett.* 83 (2002) 37.
- [6] Y. Segura, P. Cool, P. Kustrowski, L. Chmielarz, R. Dziembaj, E.F. Vansant, *J. Phys. Chem. B* 109 (2005) 12071.
- [7] D.A. Ruddy, N.L. Ohler, A.T. Bell, T.D. Tilley, *J. Catal.* 238 (2006) 277.
- [8] C. Hess, I.J. Drake, J.D. Hoefelmeyer, T.D. Tilley, A.T. Bell, *Catal. Lett.* 105 (2005) 1.
- [9] C. Hess, M.H. Looi, S.B. Abd Hamid, R. Schlögl, *Chem. Commun.* (2006) 451.
- [10] Q. Sun, J.M. Jehng, H.H. Hu, R.G. Herman, I.E. Wachs, K.J. Klier, *J. Catal.* 165 (1997) 91.
- [11] S. Iruata, L.M. Cornaglia, E.E. Miro, E.A. Lombardo, *J. Catal.* 156 (1995) 167.
- [12] D.S. Kim, J.A. Tatibouet, I.E. Wachs, *J. Catal.* 136 (1992) 209.
- [13] G. Deo, I.E. Wachs, *J. Haber, Crit. Rev. Surf. Chem.* 40 (1994) 1.
- [14] J.-M. Jeng, H. Hu, X. Gao, I.E. Wachs, *Catal. Today* 28 (1996) 335.
- [15] M. Banares, X. Gao, J.L.G. Fierro, I.E. Wachs, *Stud. Surf. Sci. Catal.* 110 (1997) 295.
- [16] B. Jonson, B. Rebenstorf, R. Larsson, S.L. Andersson, *J. Chem. Soc. Faraday Trans.* 84 (1988) 1897.
- [17] (a) M. Schraml-Marth, A. Wokaun, M. Pohl, H.L. Krauss, *J. Chem. Soc. Faraday Trans.* 87 (1991) 2635;
(b) U. Scharf, M. Schraml-Marth, A. Wokaun, A. Baiker, *J. Chem. Soc. Faraday Trans.* 87 (1991) 3299.
- [18] (a) K. Inumaru, T. Okuhara, M. Misono, N. Matsubayashi, H. Shimada, A. Nishijima, *J. Chem. Soc. Faraday Trans.* 88 (1992) 625;
(b) K. Inumaru, T. Okuhara, M. Misono, *J. Phys. Chem.* 95 (1991) 4826;
(c) K. Inumaru, T. Okuhara, M. Misono, N. Matsubayashi, H. Shimada, A. Nishijima, *J. Chem. Soc. Faraday Trans.* 87 (1991) 1807.

- [19] S. Xie, E. Iglesia, A.T. Bell, *Langmuir* 16 (2000) 7162.
- [20] X. Gao, S.R. Bare, B. Weckhuysen, I.E. Wachs, *J. Phys. Chem. B* 102 (1998) 10842.
- [21] N. Das, H. Eckert, H. Hu, I.E. Wachs, J.F. Walzer, F.J. Feher, *J. Phys. Chem.* 97 (1993) 8240.
- [22] G.T. Went, S.T. Oyama, A.T. Bell, *J. Phys. Chem.* 94 (1990) 4240.
- [23] F. Roozeboom, M.C. Mittelmeljer-Hazeleger, J.A. Mouljin, J. Medema, V.H.J. de Beer, P.J. Gellings, *J. Phys. Chem.* 84 (1980) 2783.
- [24] G. Lische, W. Hanke, H.G. Jerschke, J. Ohlmann, *J. Catal.* 91 (1985) 54.
- [25] F. Arena, F. Frusteri, G. Martra, S. Coluccia, A. Parmaliana, *J. Chem. Soc. Faraday Trans.* 93 (1997) 3849.
- [26] (a) S. Yoshida, T. Tanaka, Y. Nishimura, H. Mizutani, T. Funabiki, *Proc. 9th Int. Congr. Catal.*, vol. 3, 1988, p. 1473;
(b) S. Yoshida, T. Tanaka, T. Hanada, T. Hiraiwa, H. Kanai, T. Funabiki, *Catal. Lett.* 12 (1992) 277;
(c) T. Tanaka, H. Yamashita, R. Tsuchitani, T. Funabiki, S. Yoshida, *J. Chem. Soc. Faraday Trans.* 84 (1988) 2987.
- [27] N.K. Nag, F.E. Massoth, *J. Catal.* 124 (1990) 127.
- [28] M.A. Eberhardt, A. Proctor, M. Houalla, D.M. Hercules, *J. Catal.* 160 (1996) 27, and references therein.
- [29] K.L. Fudjala, T.D. Tilley, *J. Catal.* 216 (2003) 265.
- [30] C. Coperet, M. Chabanas, R.P. Saint-Arroman, J.-M. Basset, *Angew. Chem.* 42 (2003) 15.
- [31] K. Zhu, Z. Ma, Y. Zou, W. Zhou, T. Chen, H. He, *Chem. Commun.* (2001) 2552.
- [32] R. Rulkens, J.L. Male, K.W. Terry, B. Olthof, A. Khadakov, A.T. Bell, E. Iglesia, T.D. Tilley, *Chem. Mater.* 11 (1999) 2966.
- [33] C. Hess, J.D. Hoefelmeyer, T.D. Tilley, *J. Phys. Chem. B* 108 (2004) 9703.
- [34] E.F. Vansant, P. Van der Voort, K.C. Vrancken, *Characterization and Chemical Modification of the Silica Surface, Studies in Surface Science and Catalysis*, vol. 93, Elsevier, Amsterdam, 1995, and references therein.
- [35] Z. Luan, J.A. Fournier, J.B. Wooten, D.E. Miser, *Micropor. Mesopor. Mater.* 83 (2005) 150.
- [36] K.C. Vrancken, P. Van der Voort, I. Gillis-D'Hamers, E.F. Vansant, P. Grobet, *J. Chem. Soc. Faraday Trans.* 88 (1992) 3197.
- [37] W.A. Carvalho, M. Wallau, U. Schuchardt, *J. Mol. Catal. A* 144 (1999) 91.
- [38] P. Roman, A. Aranzabe, A. Luque, J.M. Gutierrez-Zorilla, *Mater. Res. Bull.* 26 (1991) 731.
- [39] (a) M. Klaasen, A. Berndtsson, J. Hedman, R. Nilsson, R. Nyholm, C. Nordling, *J. Electron. Spectrosc. Relat. Phenom.* 3 (1974) 427;
(b) W.E. Morgan, J.R. Van Wazer, *J. Phys. Chem.* 77 (1973) 96;
(c) T.L. Barr, *Appl. Surf. Sci.* 15 (1983) 1.
- [40] D. Briggs, M.P. Seah, *Practical Surface Analysis*, Wiley, Chichester, 1990.
- [41] K.M.R. Kallury, P.M. Macdonald, M. Thompson, *Langmuir* 10 (1994) 492.
- [42] M.R. Horner, F.J. Boerio, H.M. Clearfield, *J. Adhes. Sci. Technol.* 6 (1992) 1.
- [43] R.J. Colton, A.M. Guzman, J.W. Rabalais, *Acc. Chem. Res.* 11 (1978) 170.
- [44] P.R. Moses, L.M. Wier, J.C. Lennox, H.O. Finklea, J.R. Lenhard, R.W. Murray, *Anal. Chem.* 50 (1978) 576.
- [45] G.A. Sawatzky, D. Post, *Phys. Rev. B* 20 (1979) 1546.
- [46] (a) S.L.T. Andersson, *J. Chem. Soc. Faraday Trans.* 75 (1979) 1356;
(b) J.A. Odriozola, J. Soria, G.A. Somorjai, H. Heinemann, J.F. Garcia de la Banda, M. Lopez Granados, J.C. Conesa, *J. Phys. Chem.* 95 (1991) 240.
- [47] G. Meunier, B. Mocaer, S. Kasztelan, L.R. LeCoustumer, J. Grimblot, J.P. Bonnelle, *Appl. Catal.* 21 (1986) 520.
- [48] C.J. Brinker, R. Kirkpatrick, D.R. Tallant, B.C. Bunker, B. Montez, *J. Non-Cryst. Solids* 99 (1988) 418.
- [49] (a) D.R. Tallant, B.C. Bunker, C.J. Brinker, C.A. Balfe, *Mater. Res. Soc. Symp. Proc.* 73 (1986) 261;
(b) R.H. Stolen, G.E. Walrafen, *J. Chem. Phys.* 64 (1976) 2623;
(c) B.C. Brinker, D.R. Tallant, E.P. Roth, C.S. Ashley, *Mater. Res. Soc. Symp. Proc.* 61 (1986) 387.
- [50] D. Lin-Vien, N.B. Colthup, W.G. Fateley, J.G. Grasselli, *The Handbook of Infrared and Raman Characteristic Frequencies of Organic Molecules*, Academic Press, Boston, 1991.
- [51] H. Okabayashi, K. Taga, K. Miyagai, T. Uehara, T. Yoshida, E. Nishio, *J. Phys. Chem.* 95 (1991) 7932.
- [52] F.D. Hardcastle, I.E. Wachs, *J. Phys. Chem.* 95 (1991) 5031.
- [53] (a) L. Abello, E. Husson, Y. Repelin, G. Lucazeau, *J. Solid State Chem.* 56 (1985) 379;
(b) Y. Repelin, E. Husson, L. Abello, G. Lucazeau, *Spectrochim. Acta* 41A (1985) 993.
- [54] I. Shimizu, H. Okabayashi, K. Taga, A. Yoshino, E. Nishio, C.J. O'Connor, *Vibr. Spectrosc.* 14 (1997) 125.
- [55] D.H. Williams, I. Fleming, *Spectroscopic Methods in Organic Chemistry*, McGraw-Hill, Maidenhead, 1989, and references therein.
- [56] This interpretation of the Raman results is supported by ²⁹Si CPMAS NMR experiments performed by Ulla Gro Nielson.